

We are IntechOpen, the world's leading publisher of Open Access books Built by scientists, for scientists

4,800

Open access books available

122,000

International authors and editors

135M

Downloads

Our authors are among the

154

Countries delivered to

TOP 1%

most cited scientists

12.2%

Contributors from top 500 universities



WEB OF SCIENCE™

Selection of our books indexed in the Book Citation Index
in Web of Science™ Core Collection (BKCI)

Interested in publishing with us?
Contact book.department@intechopen.com

Numbers displayed above are based on latest data collected.
For more information visit www.intechopen.com



The Photorefractive Effect in Liquid Crystals

*Takeo Sasaki, Khoa Van Le, Yumiko Naka
and Takafumi Sassa*

Abstract

This chapter summarizes the state of the art of research regarding photorefractive liquid crystals. Photorefractive effect is of interest because it can be used to obtain dynamic holograms, based on interference between dual laser beams within a liquid crystal to generate a refractive index grating. This technique can be employed in numerous diffraction optics applications, such as optical amplifiers, phase-conjugate wave generators, 3D displays, novelty filters, and optical tomography. The photorefractive effect in liquid crystals is especially pronounced, and both ferroelectric and nematic liquid crystals have been researched for this purpose, with the former showing special promise in practical applications. As an example, ferroelectric liquid crystals have been found to readily produce a refractive index grating in conjunction with a significant gain and a formation time of 900 ms.

Keywords: photorefractive effect, hologram, photoconductivity, nonlinear optics, optical amplification

1. Introduction

Photorefractive effect is a nonlinear optical phenomenon by which the refractive index of a medium can be modified. This effect can be used to produce rewritable, dynamic (that is, temporal) holographic images [1, 2]. Associated applications include the production of phase-conjugate beams and the amplification of optical signals. There are numerous potential uses of this effect in optical devices, such as in the fabrication of electrical transistors. As an example, the photorefractive phenomenon can result in the appearance of both electro-optic and photovoltaic properties in optically transparent materials. Numerous such substances have been reported, including organic molecular crystals, inorganic ferroelectric photoconductive crystals, amorphous organic photoconductive materials, photoconductive liquid crystals (LCs), photoconductive amphiphilic compounds, and photoconductive organic polymers [3–5]. Among these, organic compounds tend to have the shortest response times and greatest photorefractivity values, and hence these are of special interest [6]. Both electro-optic and photovoltaic mechanisms contribute to variations in refractive index that are associated with the photorefractive effect (**Figure 1**). The separation of photo-induced charges in a photorefractive substance and associated refractive index variations resulting from the electro-optic effect can produce a refractive index grating. The application of an electric field to such devices can also enhance the efficiency of charge generation. Photoconductive

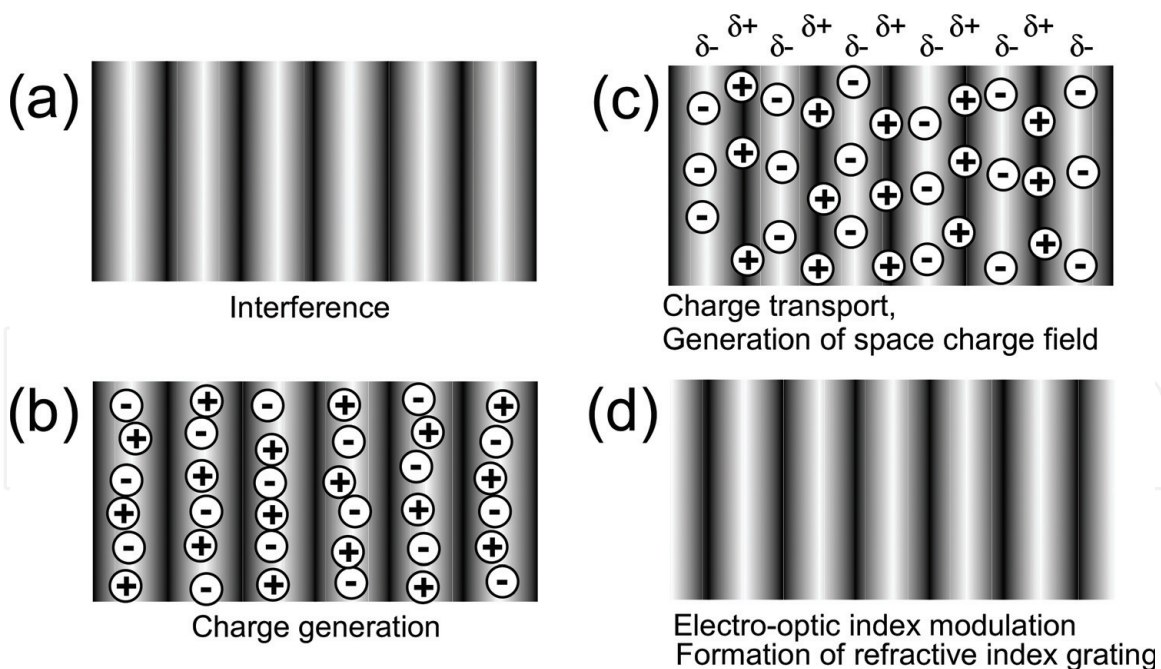


Figure 1.

A diagram summarizing the photorefractive effect mechanism. (a) Dual laser beams undergo interference in a photorefractive compound; (b) charges are produced at the light regions associated with interference fringes; (c) trap sites in the light regions hold electrons, while hole migration occurs via drift or diffusion due to an external electric field, such that an internal electric field is produced between the dark and light regions; and (d) the refractive index in specific areas is modified as a result of the internal electric field.

glassy polymers containing high levels of D- π -A chromophores (comprising π -conjugated systems with both donor and acceptor moieties) tend to exhibit especially high photorefractivity [3–7]. These materials have been suggested for use in 3D displays, real-time edge enhancement, and holographic interferometry [7]. Nevertheless, it remains necessary to reduce the electric field values of 30–50 V/ μm that must be applied to activate photorefractivity, as well as to improve the sluggish response times of these materials (approximately 100 ms). LCs, which are essentially in the liquid state and thus can be driven by the application of lower electric fields, have also been investigated with regard to their photorefractive properties [7]. Nematic LCs were reported to show photorefractivity in 1994 [8], and this effect was especially pronounced when the compounds were subjected to a low electric field (several V/ μm) [9]. Surface-stabilized ferroelectric liquid crystals (SS-FLCs) combined with photoconductive materials have also shown photorefractivity [10, 11]. Ferroelectric liquid crystals (FLCs) have a layered helical structure [12, 13] in conjunction with a chiral smectic C (SmC*) phase. Interestingly, these materials only exhibit ferroelectricity in the form of thin films (several μm in thickness) [12]. When such films are contained between the glass plates, the SmC* phase helix uncoils to generate a surface-stabilized (SS) state that shows spontaneous polarization (Ps) (**Figure 2**). Typically, a film thickness of 2 μm is employed for practical applications, such that the FLC molecules are forced into a two-dimensional SS alignment, the direction of which varies with the Ps direction (**Figure 3**). Applying an alternating electric field to the film results in an ongoing back-and-forth motion of the molecules on a time scale of less than 1 ms. The electric field determines the Ps direction, which in turn affects the properties of the film. An internal electric field can also modify the Ps direction in SS-FLCs, and **Figure 4** presents a diagram showing the photorefractive effect mechanism in an FLC. The interference between laser beams in an FLC mixed with a photoconductive material results in an internal electric field due to charge separation between dark and light regions. This field modifies the Ps direction between the dark and light locations within the

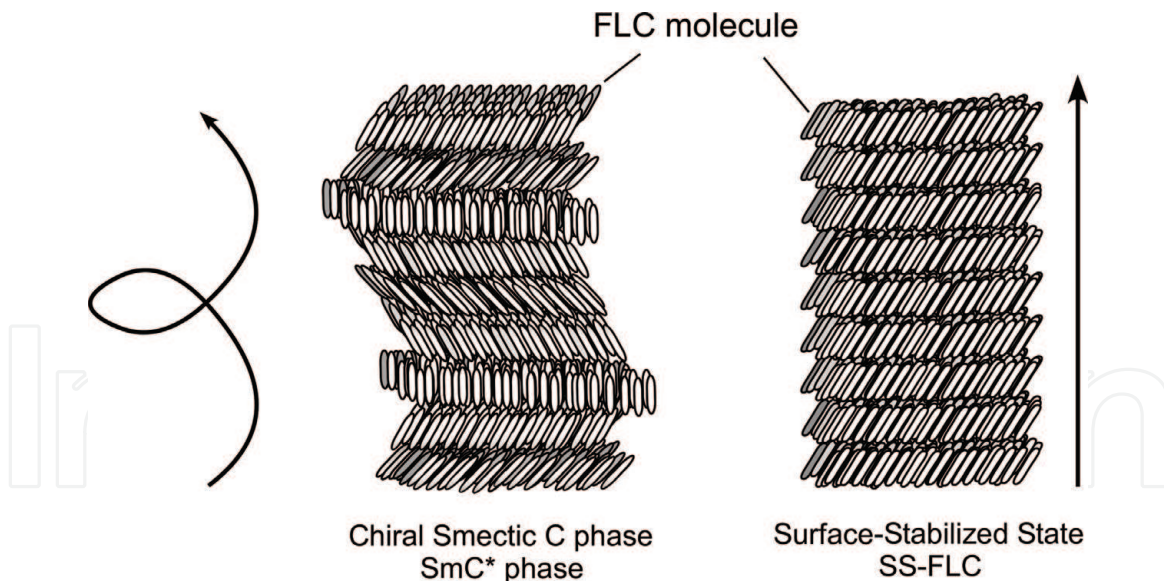


Figure 2.
SmC phase and SS state (SS-FLC) structures.

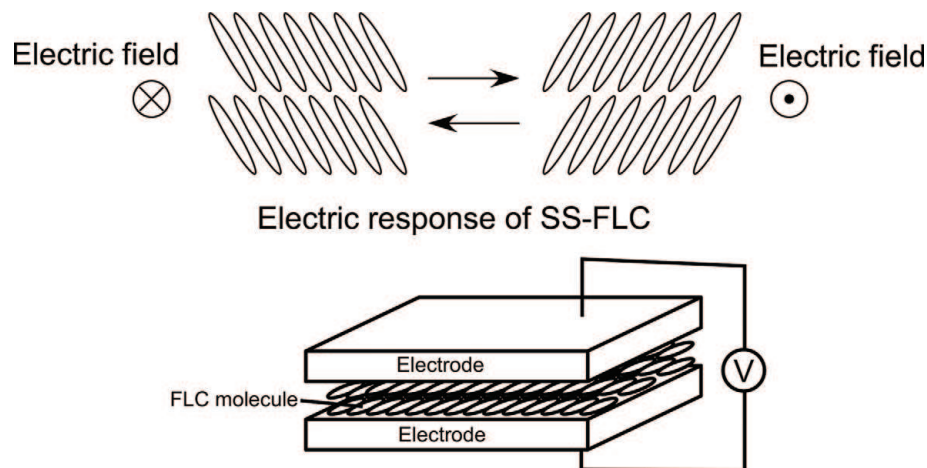
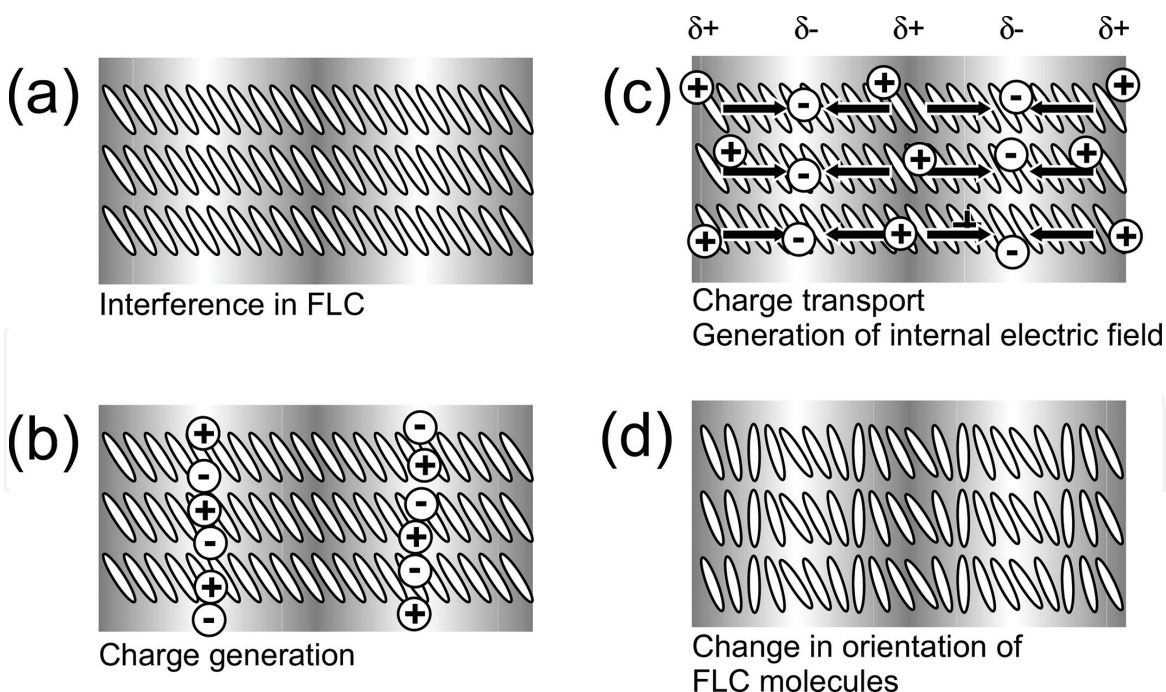


Figure 3.
Electro-optical switching of an FLC in the SS state.

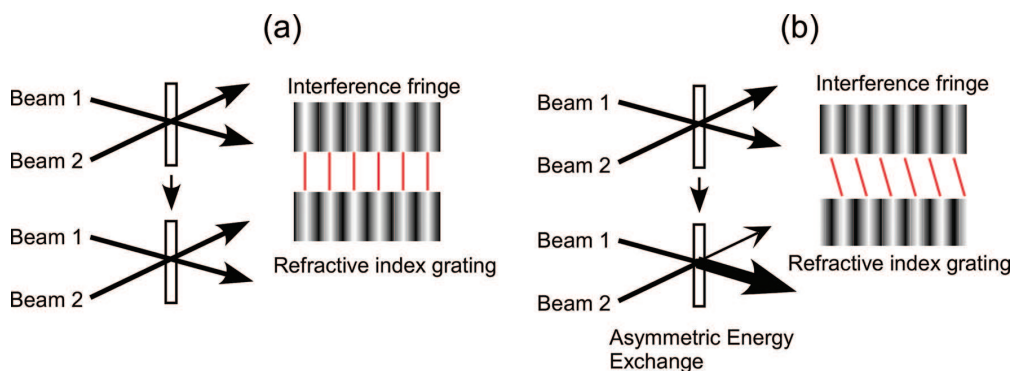
interference fringes, which in turn produces periodic variations in the FLC molecular orientation. Whereas in some organic photorefractive materials there is a bulk polarization response to the internal electric field, in the case of an FLC there is a molecular dipole response. Thus, the exceptionally rapid FLC molecular switching is a consequence of the bulk polarization response.

1.1 Characteristics of the photorefractive effect

The photorefractive effect induces variations in refractive index between the dark and light points in interference fringes. As a result, the refractive index grating phase is moved away from these fringes. In the case that one photogenerated charge is not moved from the light region, the magnitude of this shift is $\pi/2$. If a substance exhibits photochemical activity but not photorefractivity, the phasing of the resulting refractive index grating is equivalent to that of the interference fringes because only a photochemical reaction takes place at the light regions (**Figure 5a**), and this grating diffracts the laser beams. In the case that the interfering beams have the same intensity, symmetric diffraction is obtained and so there is no change in the transmission intensities of the beams. As shown in the figure, beams 1 and 2 are diffracted toward each other. In contrast, if a photorefractive material is employed,


Figure 4.

A diagram showing the FLC photorefractivity mechanism. (a) Dual laser beams undergo interference in a mixture of an FLC in the SS state with a photoconductive compound; (b) charge generation takes place within the light regions of the interference fringes; (c) trap sites in the light regions hold electrons, while holes move via drift or diffusion due to an external electric field, producing an internal electric field between the dark and light zones; (d) the spontaneous polarization vector orientation (that is, the mesogen orientation in the FLC) is modified by the internal electric field.


Figure 5.

Diagrams of refractive index grating formations. (a) Photochromic and (b) photorefractive gratings.

there is a phase shift of the grating relative to the fringes that modifies both beams. Specifically, both beams undergo energetic coupling such that beams 1 and 2 become less and more intense, respectively (**Figure 5b**). This amplification of one beam by the second beam as a result of dual-beam coupling is referred to as asymmetric energy exchange [3]. The appearance of this phenomenon, which can be applied to numerous optical devices, is characteristic of a photorefractive material.

1.2 Evaluation of photorefractivity

Dual-beam coupling is often used to assess the appearance of photorefractivity. In this technique, two beams are obtained from a p-polarized laser beam, using a beam splitter, and these beams interfere with one another inside a film specimen to which a high-voltage electric field has been applied to enhance charge generation. Variations in the intensity of the transmitted beam are tracked, and photorefractive substances will exhibit asymmetric energy exchange. The gain coefficient is

determined from changes in the beam intensity due to dual-beam coupling, and is used to communicate the magnitude of the photorefractivity. As a prerequisite to calculating this term, it is necessary to ascertain whether Bragg or Raman-Nath diffraction occurs, based on the dimensionless parameter Q , calculated as:

$$Q = 2\pi\lambda L/n\Lambda^2. \quad (1)$$

Specifically, a Q value greater than 1 indicates Bragg diffraction. In such cases, only a single diffraction order is obtained as multiple scattering does not take place. In contrast, a Q value less than 1 is associated with Raman-Nath diffraction involving numerous diffraction orders. Q values in excess of 10 ensure that solely Bragg diffraction occurs. The dual-beam coupling gain coefficient, Γ [cm^{-1}], can be calculated using the equation:

$$\Gamma = \frac{1}{D} \ln \left(\frac{gm}{1+m-g} \right) \quad (2)$$

Here, $D = L/\cos(\theta)$ is the signal beam interaction path (where L is the sample thickness and θ is the angle of beam propagation in the sample), g is the signal beam intensity behind the sample with the pump beam ratioed to that without, and m is the pump/signal intensity ratio in front of the sample [1–3].

2. Photorefractive effect of FLCs

2.1 Two-beam coupling experiments with FLCs

Research regarding the photorefractivity of commercial FLCs combined with photoconductive materials began circa 2000 [10, 11] and was continued by Sasaki et al. and Golemme et al. [7, 14]. This prior experimental work was based on dual-beam coupling trials incorporating a 488-nm Ar^+ laser, employing the photoconductive materials presented in **Figure 6** along with SCE8 (Clariant, SmC^* at 60°C , SmA at 80°C , N^* at 104°C , $\text{Ps} = 4.5 \text{ nC/cm}^2$), a combination of chiral and LC compounds, such as the FLC. In these trials, a mixture of the FLC with trinitrofluorenone (TNF, 0.1 wt.%) and carbazole diphenylhydrazone (CDH, 2 wt.%) was injected into a 10- μm gap in a glass cell having an alignment layer composed of polyimide and 1 cm^2 indium tin oxide electrodes (**Figure 7**). The typical asymmetric energy exchange obtained upon applying a 0.1 V/ μm DC electric field to an FLC (SCE8)/CDH/TNF specimen is presented in **Figure 8** [15]. In these trials, one beam exhibited enhanced transmittance while the other showed reduced intensity following interference within the FLC, resulting in symmetric variations in the transmitted intensities. These results demonstrate that a refractive index grating was

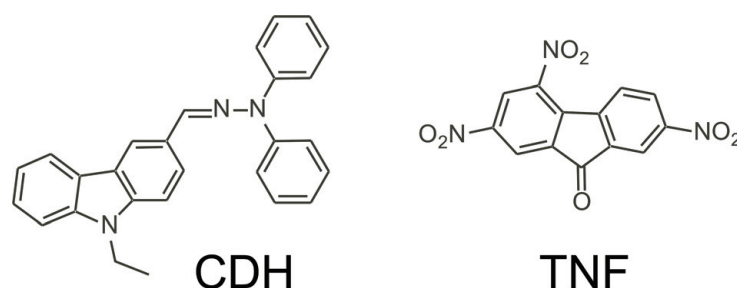


Figure 6.
Molecular structures of the photoconductive chemical CDH and the sensitizer (that is, electron trap) TNF.

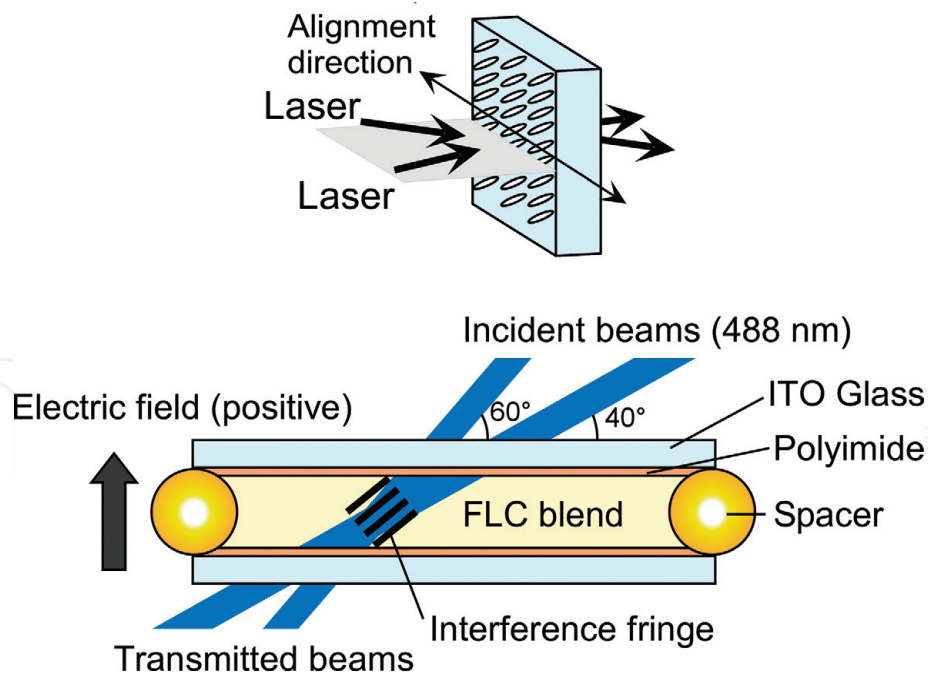


Figure 7.
The structure of an LC cell and the associated laser beam incidence.

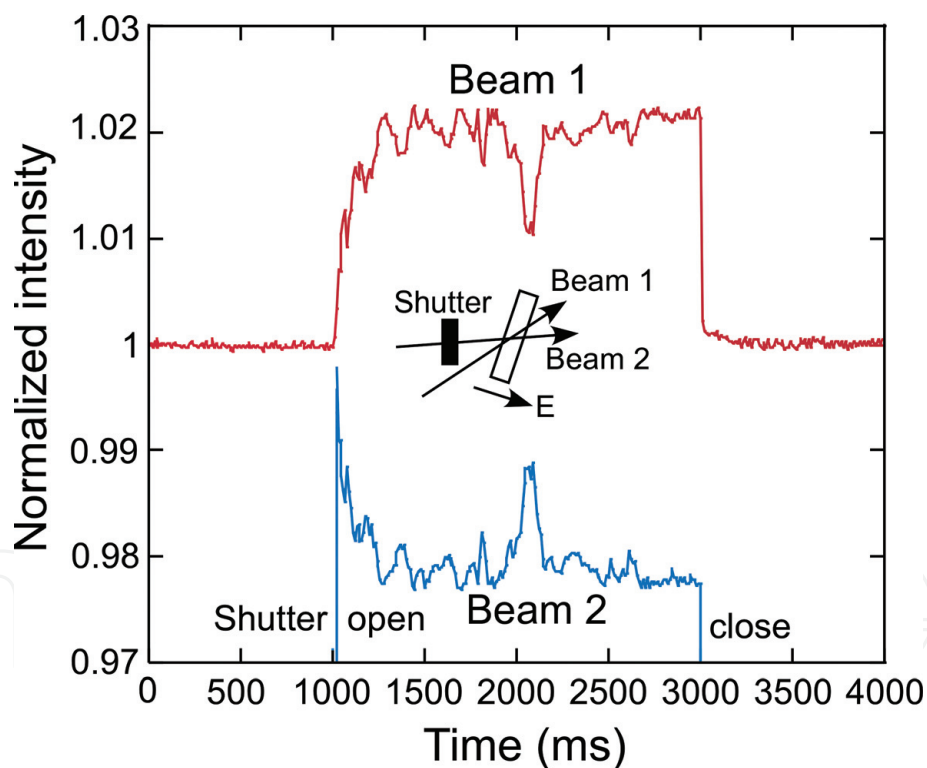


Figure 8.
A typical asymmetric energy exchange obtained within the FLC SCE8 when combined with 2 wt.% CDH and 0.1 wt.% TNF and having an applied electric field of $+0.3 \text{ V}/\mu\text{m}$.

generated at the interference fringes in conjunction with a phase shift. This grating was associated with Bragg diffraction, without any higher-order diffractions.

Figure 9a summarizes the effects of temperature on the gain coefficient of SCE8 containing 0.1 and 2 wt.% TNF and CDH, respectively. In this system, temperatures less than 46°C were required to realize asymmetric energy exchange. **Figure 9b** plots the effects of temperature on the spontaneous polarization of an equivalent specimen and demonstrates a loss of polarization at the same temperature. These data demonstrate that the sample had to be within the SmC^* phase temperature

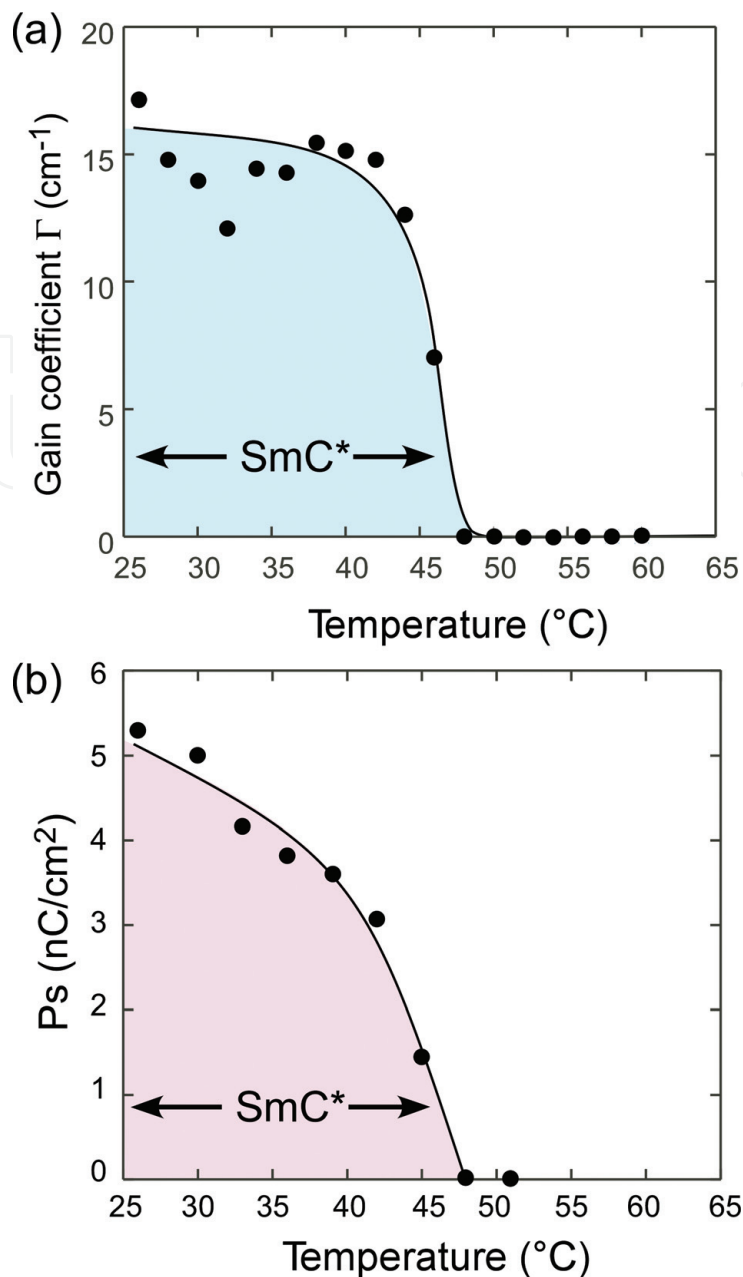


Figure 9. The effect of temperature on (a) the gain coefficient and (b) the spontaneous polarization of the FLC SCE8 when combined with 2 wt.% CDH and 0.1 wt.% TNF. During these dual-beam coupling trials, a 0.1 V/ μ m electric field was applied.

range (that is, it had to exhibit ferroelectric properties) for the asymmetric energy exchange to appear. An FLC in the N* or SmA phase cannot undergo significant variations in molecular axis orientation in response to an internal electric field because the molecular dipole moments are perpendicular to the molecular axis and have small magnitudes. In contrast, an internal electric field can result in spontaneous polarization associated with dipole reorientation in the SmC* phase. The spontaneous polarization also causes the orientation of FLC molecules in the corresponding area to change accordingly. The data show that this specimen exhibited a maximum resolution of 0.8 μ m [15].

2.2 Effect of the applied electric field strength on the gain coefficient

The external applied electric field strength has a significant effect on photorefractive polymers and acts to promote photorefractivity by enhancing the efficiency of charge separation. Several tens of volts per μ m are necessary, and so a

typical film thickness of 100 μm requires several kilovolts. However, much weaker fields can induce photorefractivity in FLCs. As an example, an SCE8 film will exhibit its largest possible gain coefficient in conjunction with a field strength in the range of 0.2–0.4 $\text{V}/\mu\text{m}$. As such films are often 10- μm thick, a field of just several volts is sufficient. **Figure 10** plots the effect of the electric field strength on the gain coefficient for an FLC(SCE8)/CDH/TNF specimen. SCE8 containing 0.5–1 wt.% CDH exhibited a coefficient that increased along with the field strength, while the addition of 2 wt.% CDH resulted in a lower coefficient at field strengths above 0.4 $\text{V}/\mu\text{m}$. Increasing the field strength to 0.2 $\text{V}/\mu\text{m}$ promoted the generation of an oriented grating due to charge separation, but zigzag defects became evident in the SS state at higher field values, which would be expected to lower the gain coefficient due to light scattering. As of 2004, the gain coefficients reported for FLC-based specimens were significantly lower [15] than those obtained for certain polymers.

2.3 The effect of applied electric field strength on response time

Both charge separation and reorientation are associated with refractive index grating formation. Both of these processes help determine the time required to form the index grating, meaning the photorefractivity response time, and can potentially determine the rate of formation. A simple single-carrier photorefractivity model was employed to assess the time required for the formation of a refractive index grating in SCE8 [1, 2], incorporating an exponential gain transient. A single exponential function was used to fit the increases in the diffraction beam signal, written as:

$$\gamma(t)-1 = (\gamma-1)[1-\exp.(-t/\tau)]^2. \quad (3)$$

Here $\gamma(t)$ is the intensity of the transmitted beam at time t ratioed to the initial intensity (that is, $\gamma(t) = I(t)/I_0$), while τ is the time required for grating formation. **Figure 11** plots the effect of the external electric field strength on the formation

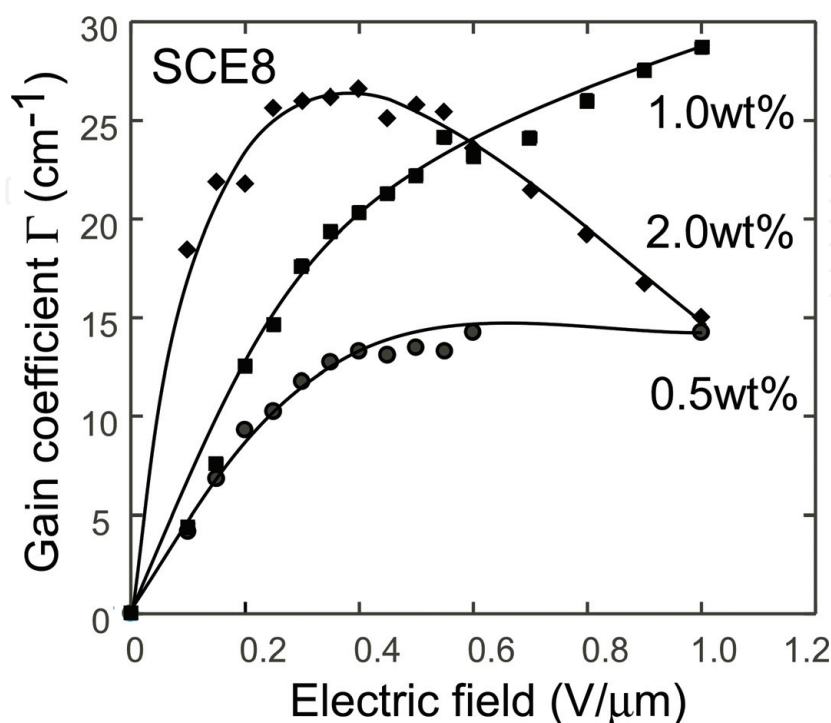


Figure 10.

The effect of electric field strength on the gain coefficient of the FLC SCE8 when combined with CDH at various concentrations and 0.1 wt.% TNF at 30°C in a cell having a 10- μm gap.

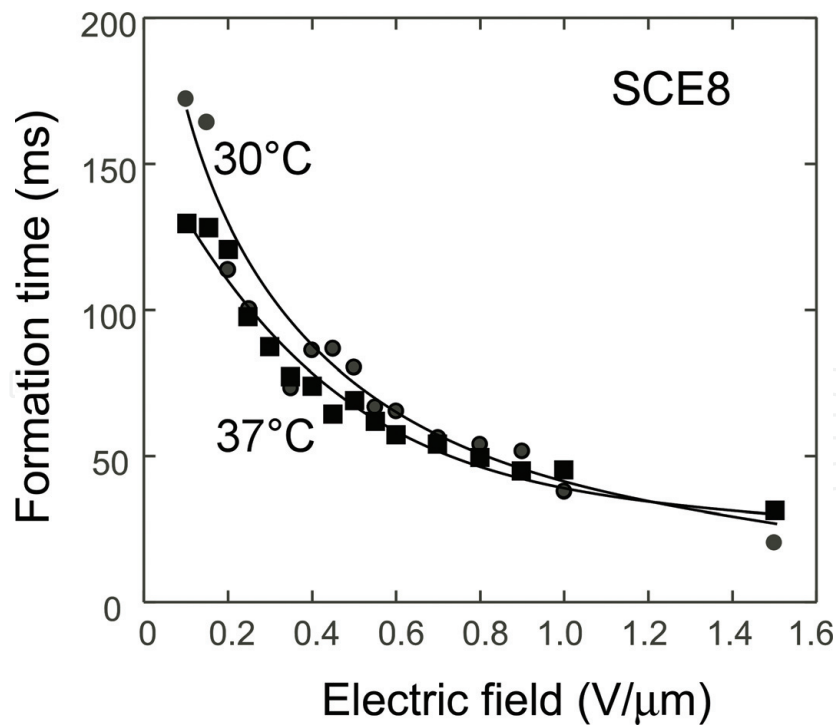


Figure 11.

The effect of electric field on the index grating formation time of the FLC SCE8 when combined with 2 wt.% CDH and 0.1 wt.% TNF in a dual-beam coupling trial. Legend: ● = data acquired at 30°C ($T/T_{SmC^*} - SmA = 0.95$); ■ = data acquired at 36°C ($T/T_{SmC^*} - SmA = 0.97$).

time for an SCE8/CDH/TNF sample and demonstrates that raising the field strength reduces the formation time, as a consequence of more efficient charge generation. Elevated temperatures also shorten the formation time, due to the lower viscosity of the material. At 30°C, the SCE8 exhibited a response time of 20 ms, which is much shorter than the typical 100 ms time span observed for polymers [7].

3. Photorefractive FLC blends

3.1 Pronounced photorefractivity of FLC blends doped with photoconductive chiral compounds

Prior to 2011, FLCs in the SS state tended to contain defects when combined with photoconductive materials. These defects reduced the photoreactivity of the mixtures due to scattering of the laser beam, and so new photorefractive FLC mixtures were researched, based on the synthesis of chiral photoconductive additives and subsequent mixing with SmC LCs. **Figure 12** shows one such blend based on an FLC [16]. In this case, the chiral photoconductive compound 3T-2 MB was added to an SmC LC together with TNF as a sensitizer, and the resulting dual-beam coupling signal acquired at 30°C is presented in **Figure 13**. Pronounced coupling was obtained in these trials, such that greater than 40% of the energy of the first laser beam was absorbed by the second beam when using a 10-μm-thick FLC film. **Figure 14a** summarizes the effect of the electric field strength on the gain coefficients. These data demonstrate that a low field strength of 1.9 V/μm resulted in a gain coefficient in excess of 1200 cm⁻¹ in the case of the 10 wt.% specimen. Relative to the values for FLCs in Section 2.2, this represents a 45-fold increase, and is ascribed to both the greater photoconductivity of this mixture and its improved transparency. In the case of photorefractive applications, the ability to induce photorefractivity in an FLC using only a low electric field is beneficial. **Figure 14b**

shows that increasing the field strength also reduced the response time, by providing more efficient charge separation, with a field strength of $1.9 \text{ V}/\mu\text{m}$ giving a formation time less than 1 ms. Both this rapid response and significant gain would assist in realizing applications such as distance measurement devices and real-time image amplifiers.

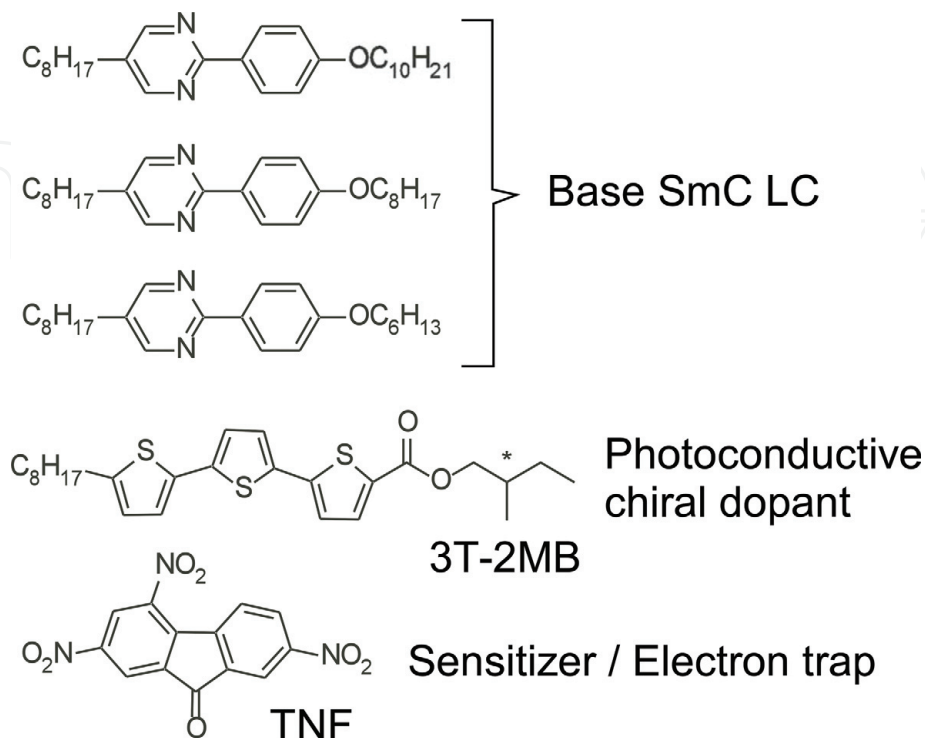


Figure 12. A photorefractive FLC sample combined with a ternary mixture of smectic LCs.

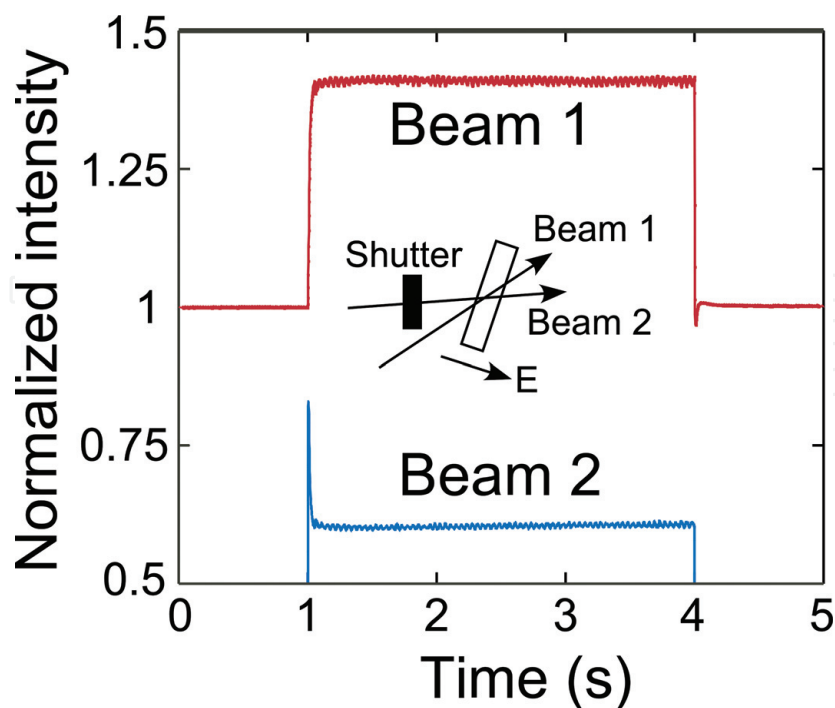


Figure 13. Typical data obtained at 30°C from dual-beam coupling trials using a mixture of a base LC, 3T-2 MB, and TNF.

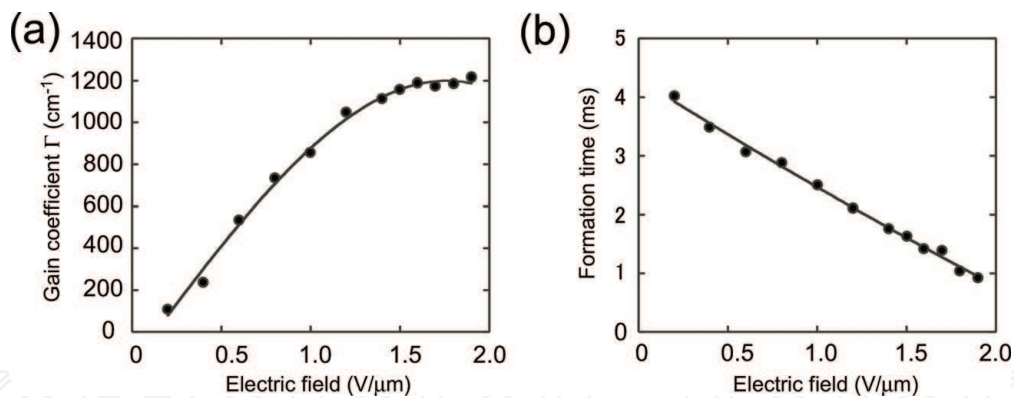


Figure 14. (a) The effect of electric field on the gain coefficients of mixtures of a base LC, 3T-2 MB (2–10 wt.%), and TNF (0.1 wt.%) at 30°C. (b) The formation times for refractive index gratings (that is, response times) for these same mixtures at 30°C.

3.2 Formation of dynamic holograms in FLC blends

A photorefractive FLC mixture has been demonstrated to form a dynamic hologram [17], such that a spatial light modulator (SLM) could be used to display a computer-generated animation. In this prior work, the SLM was exposed to a diode-pumped solid-state (DPSS) laser beam (at 488 nm) such that the FLC received the reflected beam. This beam underwent interference with a reference beam in the FLC and a refractive index grating based on Raman-Nath diffraction was generated. In other trials, a He-Ne laser beam (at 633 nm) was applied to the FLC to produce diffraction and a moving animation was generated in the diffraction (see **Figure 15**). Because image retention was not observed, the holographic image (that is, the refractive index grating) in the FLC was evidently rewritten at a rate sufficient to adequately reproduce the movie.

3.3 Dynamic amplification of optical images in photorefractive FLC blends

The photorefractive phenomenon has an obvious application in the amplification of optical signals, and this is a vital component of various optical techniques. This effect permits selective amplification, in contrast to the more well-known effects associated with lasers and nonlinear optics. Because photorefractivity results in the generation of a hologram in a material, a particular light signal can be distinguished from other signals on the basis of variations in phase, polarization, and wavelength. As an example, a photorefractive FLC mixture has demonstrated the ability to dynamically amplify a moving optical signal [16]. In this work, a rotating image (30 fps) was shown on an SLM via irradiation with a 473-nm beam such that the FLC was irradiated by the reflected beam, followed by interference with a pump beam. In these trials, amplification of the laser beam carrying the moving image was accomplished using the incident pump beam (**Figure 16**) and the signal beam intensity was increased by a factor of six. These data demonstrate that the speed of the photorefractive FLC response was such that the moving image could be amplified. It should be noted that this would not have been possible based on the average response time of a photorefractive polymer (about 100 ms). In such cases, the still image would be amplified, but not the moving image intensity.

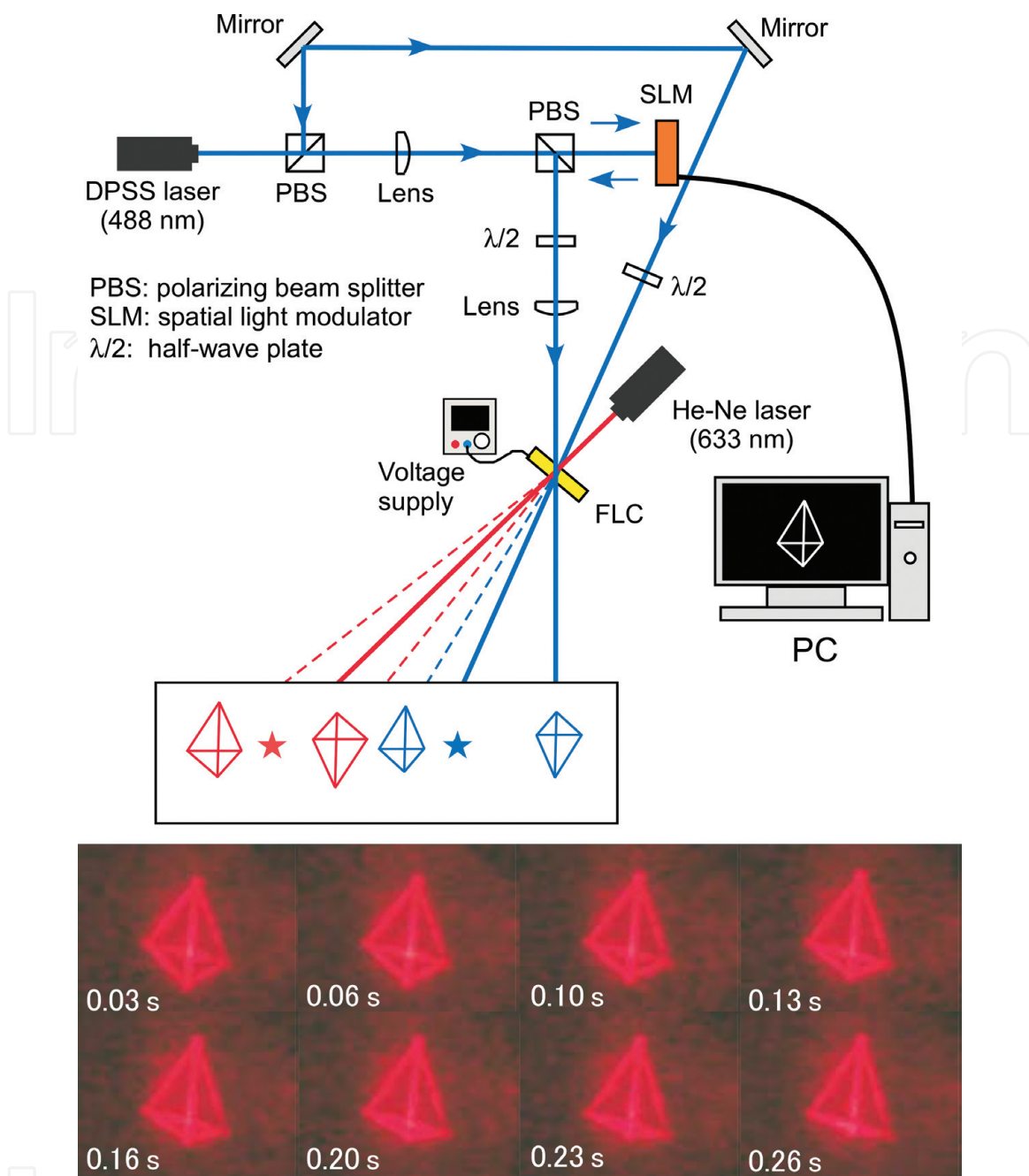


Figure 15. The formation of a dynamic hologram using an FLC, displaying a computer-generated animation on the SLM. Here, the SLM modulates the 488-nm object beam that irradiates the FLC and interferes with a reference beam. A 633-nm readout beam irradiates the FLC to generate diffraction.

3.4 Photochemical durability of photorefractive ferroelectric liquid crystal blends with chiral terthiophene photoconductive dopants

There has been research regarding the robustness of photorefractive FLC mixtures with chiral terthiophene photoconductive additives [18], and **Figure 17** plots the gain coefficient of a blend with 3T-2 MB against irradiation time. These data demonstrate a rapid drop in the gain coefficient, to the extent that only 20% of the original value remains after 90 min. This decay can possibly be attributed to a photochemical reaction of the 3T-2 MB, based on dimerization or polymerization of the terthiophene chromophore in response to irradiation. The resulting products would be expected to be insoluble in the FLC, thus degrading the photorefractivity. Such reactions could potentially be inhibited based on steric hindrance effects, and so a series of analogs was prepared: 3T-2 MB, 3-Me-3T-2 MB, 3'-Me-3T-2 MB,

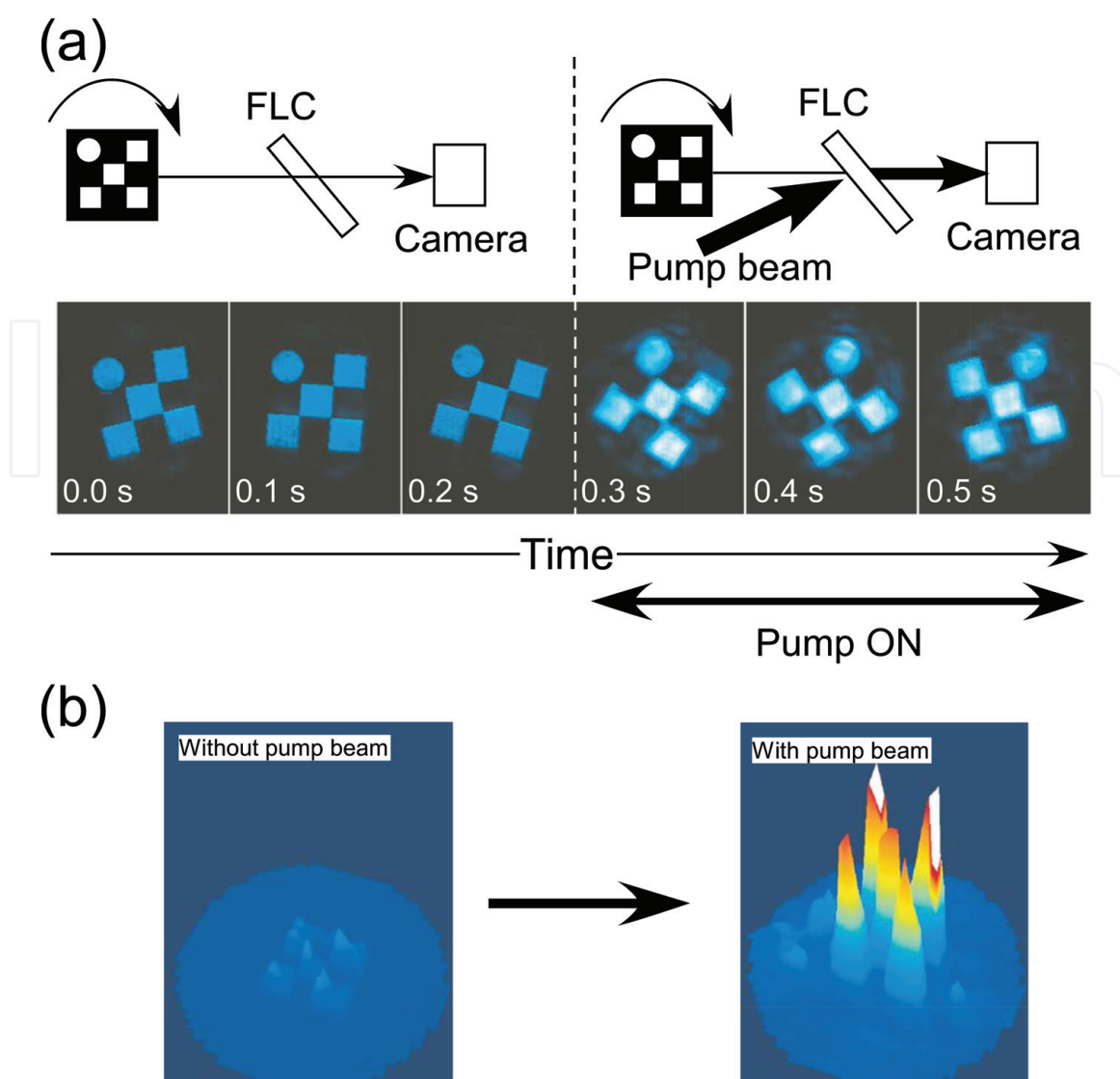


Figure 16.

(a) A demonstration of optical image amplification, in which an SLM displays a computer-generated animation. The SLM modulates a 473 nm object beam that irradiates an FLC then interferes with a reference beam. A CCD camera monitors the image sent via the FLC sample containing 10 wt.% 3T-2MB. (b) Change in signal intensity.

3''-Me-3T-2 MB and 3',3''-Me-3T-2 MB (Figure 18). Figure 19 summarizes variations in the gain coefficients of the resulting blends with irradiation time. Interestingly, the decay profiles were unchanged by varying the degree of steric hindrance in the dopant, despite expectations that methyl substituents would hinder access to the reaction site as well as the approach to the terthiophene moieties. Consequently, the loss of photorefractivity evidently was not due to dimerization or polymerization. Additional analyses of a 3T-2 MB specimen via ^1H NMR, infrared and UV-visible spectroscopy following exposure to 488-nm light found no reaction or degradation of the terthiophene moiety. Based on these results, it appears that the loss of photorefractivity resulted from factors other than those described above.

When a DC field is applied, the photorefractive gain has been shown to decay as the irradiation time is prolonged. This phenomenon was assessed by a dual-beam coupling trial employing a decayed sample stored under dark conditions. Figure 20 presents the original gain signal following laser irradiation for 60 min, after which the specimen was maintained in darkness for 12 h in the absence of an electric field. In this trial, 85% of the initial signal was recovered, demonstrating that the loss of the photorefractive effect was due to changes in the material that were reversible. The observed recoverable loss in gain can possibly be attributed to the formation of

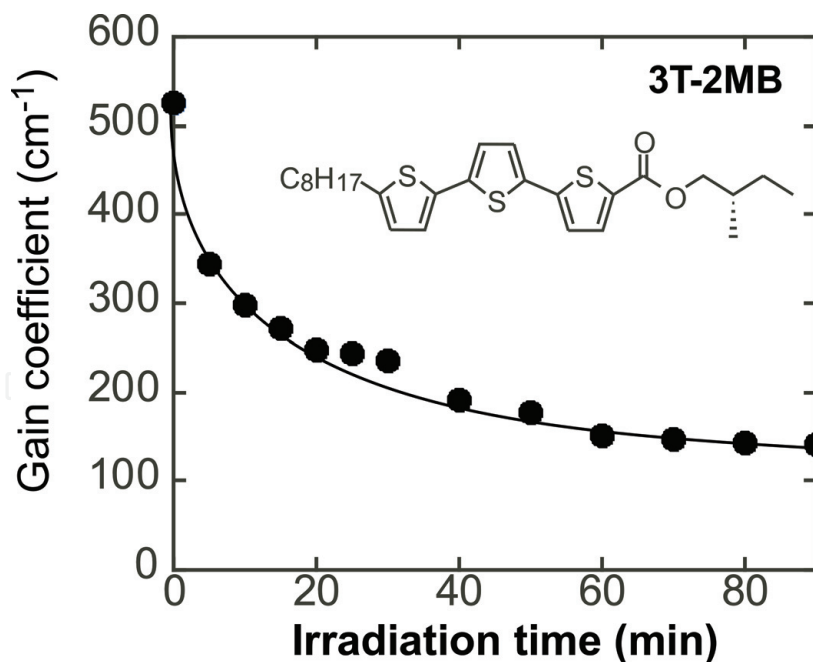


Figure 17. Molecular structures of the smectic LCs 8PP8 and 8PP10, chiral photoconductive dopants and TNF, an electron trap reagent.

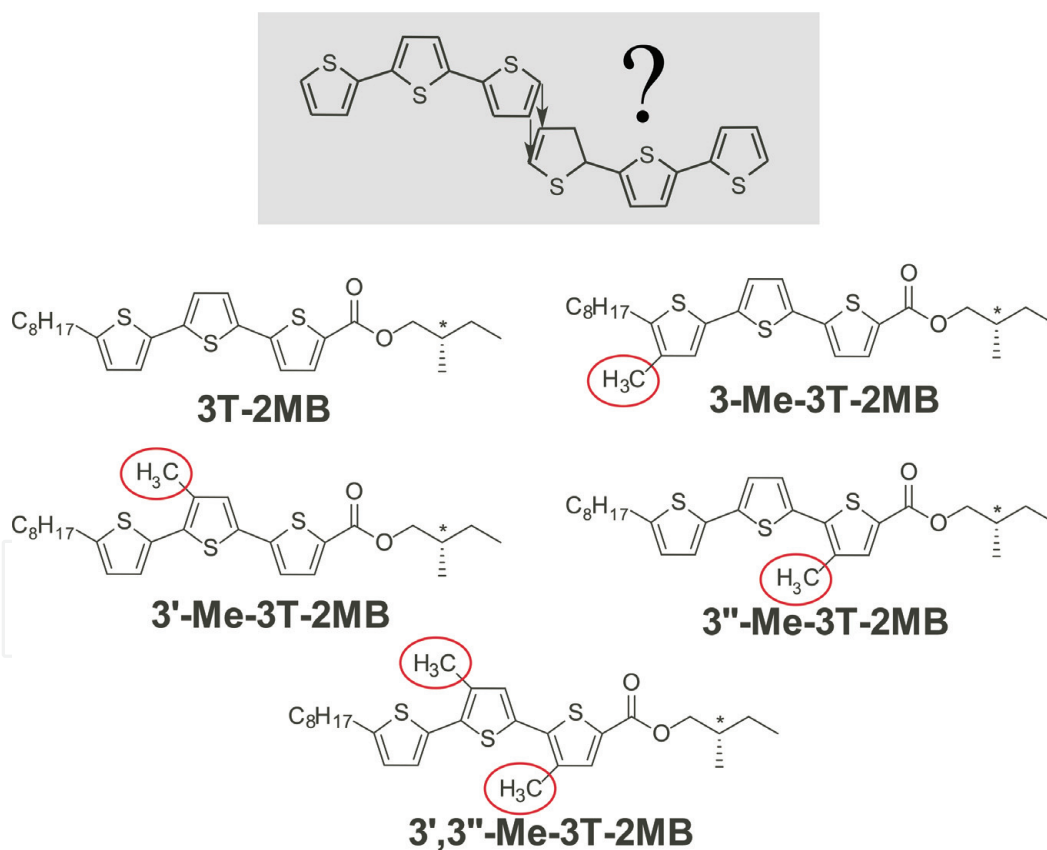


Figure 18. Variations in the gain coefficient of FLC with 6 wt.% 3T-2 MB and 0.1 wt.% TNF over time.

photogenerated ions that adhere to the indium tin oxide (ITO) electrode. It is known that charge transfer between the TNF and terthiophene occurs in response to 488-nm laser light to produce corresponding cations and anions, and these species may migrate to the electrode in response to the electric field. This process extracts ions from the LC phase, reducing its conductivity. Thus, the observed loss of photorefractivity could possibly be mitigated by employing a bipolar electric field, to reverse the direction of

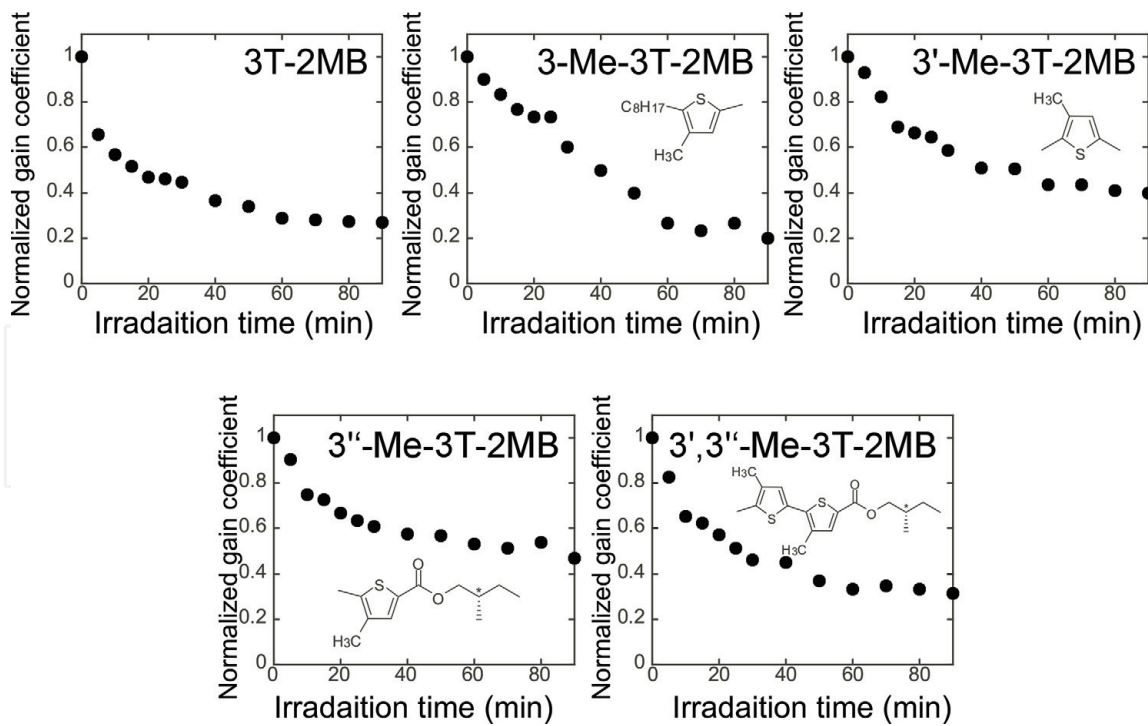


Figure 19. Variations in the gain coefficients of FLC mixed with 6 wt.% various photoconductive chiral additives and 0.1 wt.% TNF over time.

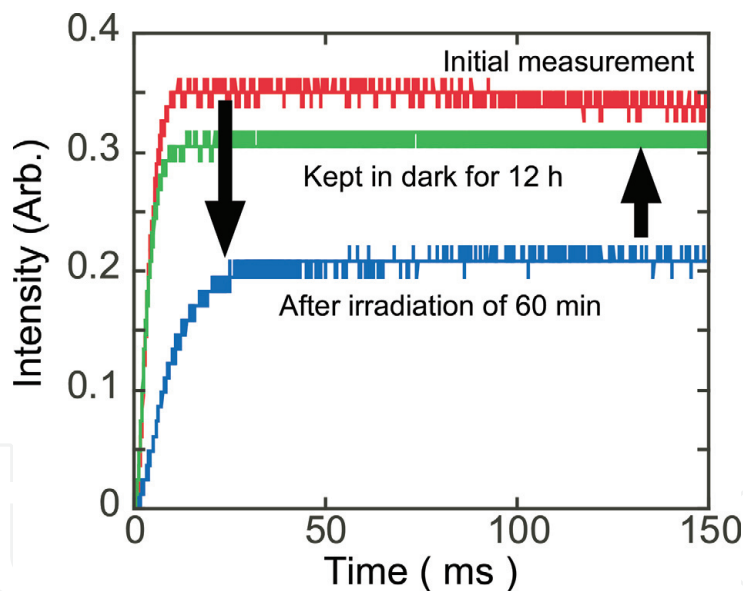


Figure 20. The dual-beam coupling signals generated by FLC doped with 3T-2 MB. The initial signal following 60 min of irradiation by laser beam (250 mW/cm^2) and the signal after storage in darkness for 12 h are shown.

migration of the photogenerated ions such that they move away from the electrode. Of course, it would be necessary to select an optimal frequency for this bipolar field based on ion mobilities, as well as to optimize the field strength. **Figure 21** presents decay profiles of the gain coefficients in conjunction with a bipolar field, and demonstrates that 80% of the original gain was retained under these conditions. These results help to confirm that the observed loss of photorefractivity in the FLC samples is due to ionic migration. The TNF anions and 3T-2 MB cations would be expected to migrate at different rates as a result of the difference in their sizes, and so the electric field strength and shape could be further tuned. In fact, the electric fields employed in present-day LC displays are somewhat complex bipolar fields rather than DC fields.

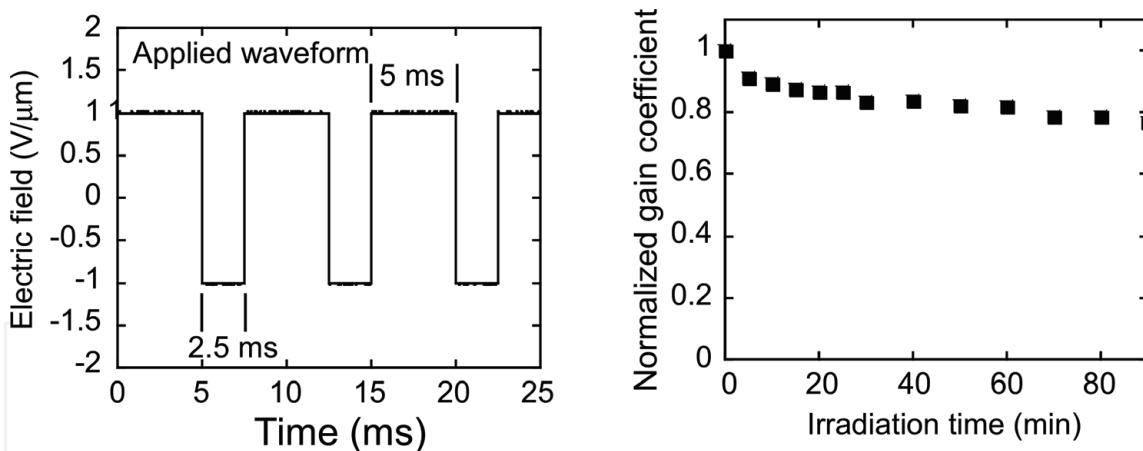


Figure 21. Variations in the gain coefficients of an FLC mixed with 6 wt.% 3 T-2 MB and 0.1 wt.% TNF over time in the presence of a bipolar electric field.

This is required in order to inhibit the adsorption of ions and the LC molecules themselves so as to prevent image sticking. Thus, the use of bipolar fields is already an important aspect of photorefractive LC devices.

3.5 Photorefractive effects in FLC blends containing extended π -conjugated compounds

The photorefractivities of terthiophene derivatives as chiral photoconductive additives have been examined at 488 nm. The practical application of FLCs in

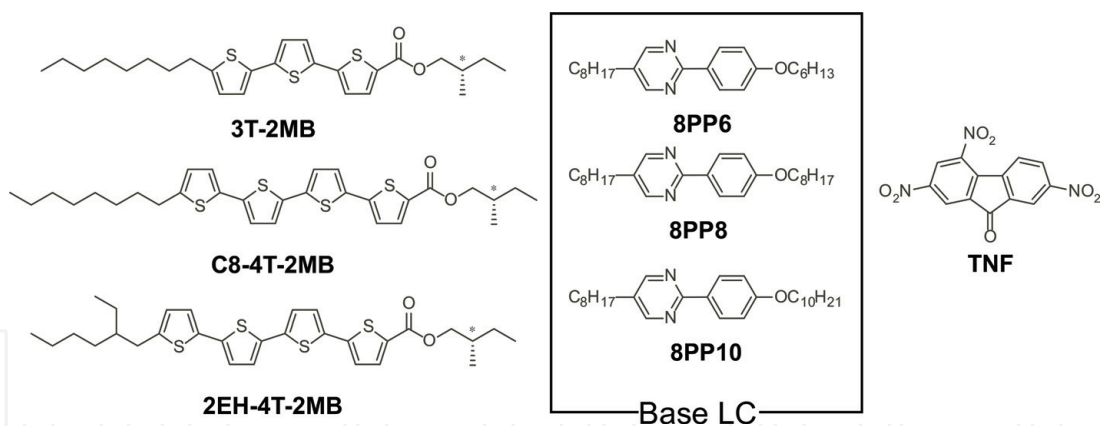


Figure 22. Molecular structures of the chiral photoconductive additives, smectic LCs, and TNF, an electron trap reagent.

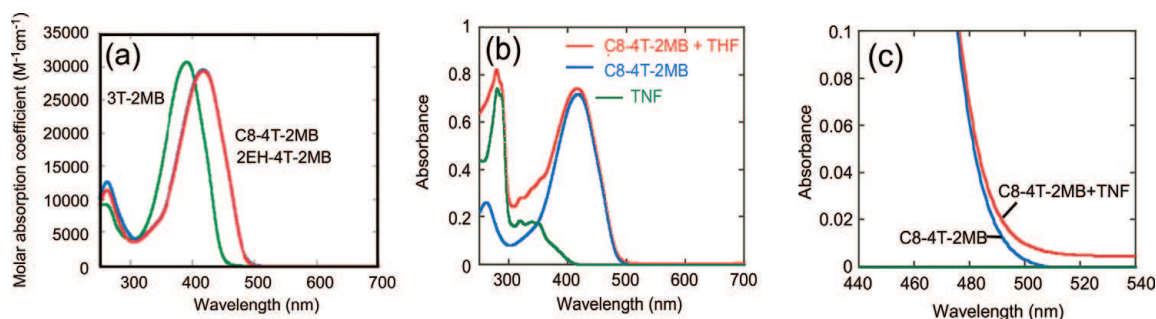


Figure 23. (a) The UV-vis absorption spectra generated by chloroform solutions of the chiral photoconductive additives C8-4T-2 MB, 2EH-4T-2 MB and 3 T-2 MB; (b) the UV-vis spectra of a chloroform solution of C8-4T-2 MB and TNF; (c) the UV-vis spectrum of C8-4T-2 MB compared to that of C8-4T-2 MB and TNF (all in chloroform solutions).

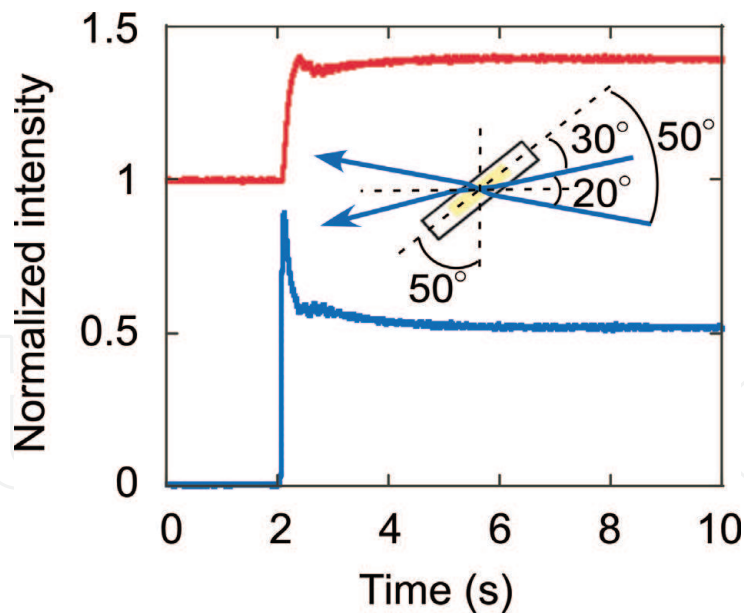


Figure 24.
 A typical asymmetric energy exchange obtained from a dual-beam coupling experiment at 30°C using a combination of a base-LC, 2EH-4T-2 MB, and TNF. Pump beam incidence occurred at the 2-s mark. The beam incidence parameters are given in the figure.

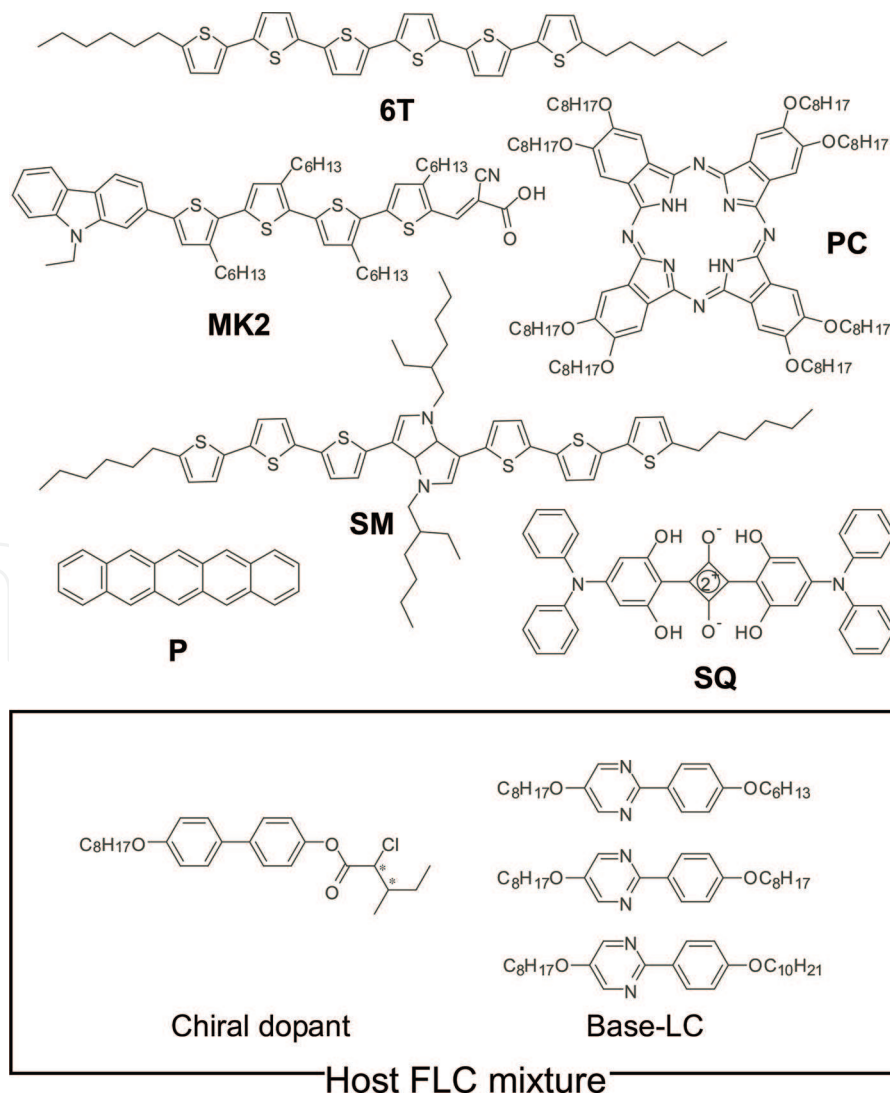


Figure 25.
 Molecular structures of the host FLC and the photoconductive compounds used in the work described herein. The chiral dopant was added at a concentration of 10 wt.% relative to the total mass of the 2:1:1 ternary mixture.

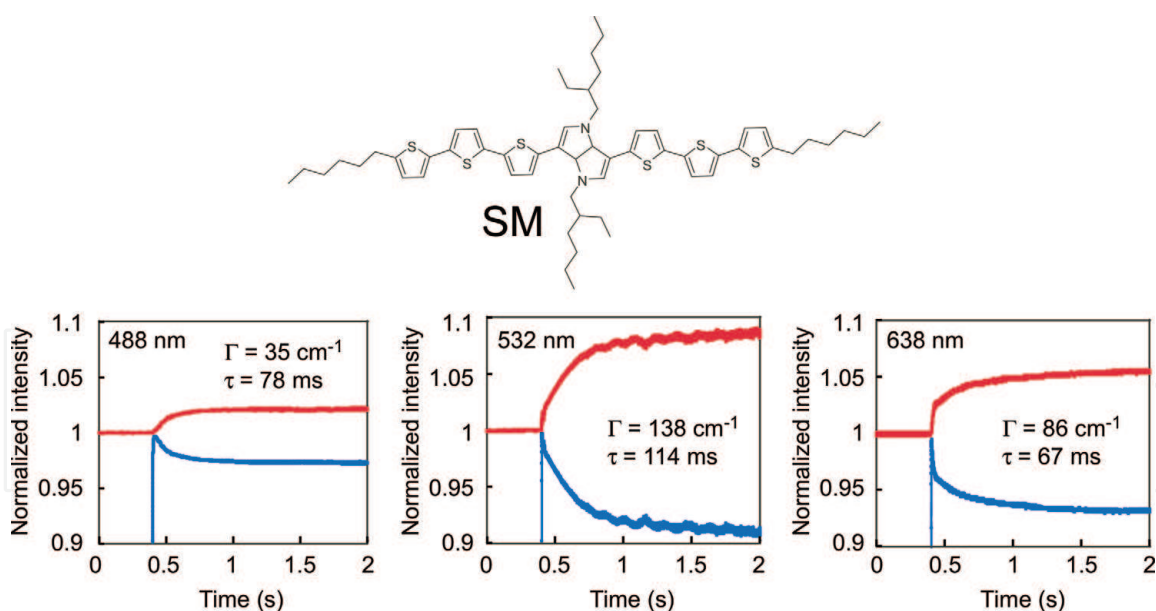


Figure 26. Asymmetric energy exchanges in an FLC mixture in which the photoconductive compound SM is present at less than 1 wt.%.

ultrasound imaging and photoacoustic interferometry requires sensitivity at longer wavelengths. Thus, chiral compounds such as those containing quarter-thiophene chromophores and sexithiophenes, as well as more complex molecular structures, have been synthesized (Figure 22). The photorefractivity of mixtures of FLCs with these dopants at longer wavelengths has also been assessed [19]. The addition of TNF to a quarter-thiophene was found to result in absorption at longer wavelengths (Figure 23) due to the formation of a charge transfer absorption band, allowing these materials to be employed in conjunction with a 532-nm writing beam. Dual-beam trials were subsequently employed to examine the photorefractivity of the resulting FLC blends. Figure 24 shows typical data for the asymmetric energy exchange in a 2EH-4 T-2 MB specimen in conjunction with a 532-nm writing beam wavelength.

Photoconductive materials having longer absorption wavelengths were additionally investigated (Figure 25). In these trials, the photoconductive compounds were mixed with a base FLC and a chiral additive. Most of the materials listed in Figure 25 could not be dissolved in the FLC, with the exception of the SM, which could be added at levels up to 1 wt.%. Thus, a blend containing 1 wt.% SM was employed for dual-beam coupling trials (Figure 26), in conjunction with continuous laser irradiation at 488, 532, and 638 nm. This sample exhibited asymmetric energy exchange even at the longest wavelength, albeit with a slow response and minimal gain. The generation of a space charge field at the interference fringes evidently involved ionic conduction, which was reflected in the slow response.

4. Conclusions

LCs are exceptionally birefringent and thus produce a significant photorefractive effect, although they suffer from light scattering due to heterogeneous molecular orientations. Smectic LCs show more pronounced photorefractivity, especially in the case of the bulk (or spontaneous) polarization of FLCs combined with photoconductive compounds. These mixtures exhibit photorefractivity solely in the ferroelectric phase and with reduced response times relative to those obtained from nematic

LCs. The various properties of FLCs, including spontaneous polarization, phase transition temperature, viscosity and SS-state homogeneity, all greatly affect photorefractivity. Both the time required for formation of a refractive index grating (that is, the response time) and the gain coefficient are significantly affected by the last factor, and so extreme homogeneity is required in a photorefractive device. Finally, FLC blends have exhibited sensitivity to wavelengths up to 638 nm following doping with photoconductive compounds.

IntechOpen

Author details


Takeo Sasaki^{1*}, Khoa Van Le¹, Yumiko Naka¹ and Takafumi Sassa²

¹ Tokyo University of Science, Tokyo, Japan

² Photonics Control Technology Team, RIKEN Center for Advanced Photonics, RIKEN Laser Science Laboratory, Wako, Japan

*Address all correspondence to: sasaki@rs.kagu.tus.ac.jp

IntechOpen

© 2018 The Author(s). Licensee IntechOpen. This chapter is distributed under the terms of the Creative Commons Attribution License (<http://creativecommons.org/licenses/by/3.0>), which permits unrestricted use, distribution, and reproduction in any medium, provided the original work is properly cited. 

References

- [1] Solymar L, Webb JD, Grunnet-Jepsen A. *The Physics and Applications of Photorefractive Materials*. Oxford: New York; 1996
- [2] Yeh P. *Introduction to Photorefractive Nonlinear Optics*. New York: Wiley; 1993
- [3] Moerner WE, Silence SM. Polymeric photorefractive materials. *Chemical Reviews*. 1994;**94**:127-155
- [4] Ostroverkhova O, Moerner WE. Organic photorefractives: Mechanisms, materials, and applications. *Chemical Reviews*. 2004;**104**:3267-3314
- [5] Sasaki T. Photorefractive effect of liquid crystalline materials. *Polymer Journal*. 2005;**37**:797-812
- [6] Meerholz K, Volodin BL, Kippelen B, Peyghambarian N. A photorefractive polymer with high optical gain and diffraction efficiency near 100%. *Nature*. 1994;**371**:497-500
- [7] Blanche PA. *Springer Series in Materials Science 240, Photorefractive Organic Materials and Applications*. Switzerland: Springer International Publishing; 2016
- [8] Khoo C, Li H, Liang Y. Observation of orientational photorefractive effects in nematic liquid crystals. *Optics Letters*. 1994;**19**:1723-1725
- [9] Ono H, Kawatsuki N. High-performance photorefractivity in high- and low-molar-mass liquid crystal mixtures. *Journal of Applied Physics*. 1999;**85**:2482-2487
- [10] Wiederrecht GP, Yoon BA, Wasielewski MR. Photorefractivity in ferroelectric liquid crystal composites containing electron donor and acceptor molecules. *Advanced Materials*. 2000;**12**:1533-1536
- [11] Sasaki T, Kino T, Shibata M, Mizusaki N, Katsuragi A, Ishikawa Y, et al. Spontaneous polarization-vector-reorientation photorefractive effect in ferroelectric liquid crystals. *Applied Physics Letters*. 2001;**78**:4112-4114
- [12] Skarp K, Handschy MA. Ferroelectric liquid crystals. Material properties and applications. *Molecular Crystals and Liquid Crystals*. 1988;**165**:439-509
- [13] Oswald P, Pieranski P. *Smectic and Columnar Liquid Crystals*. New York: Taylor & Francis; 2006
- [14] Sasaki T, Naka Y. Photorefractive effect in ferroelectric liquid crystals. *Optical Review*. 2014;**21**:99-104
- [15] Sasaki T, Mochizuki O, Noborio K, Nakazawa Y. Influence of the laser incidence conditions on the spontaneous polarization reorientation photorefractive effect of ferroelectric liquid crystals. *The Journal of Physical Chemistry. B*. 2004;**108**:17083-17088
- [16] Sasaki T, Kajikawa S, Naka Y. Dynamic amplification of light signals in photorefractive ferroelectric liquid crystalline mixtures. *Faraday Discussions*. 2014;**174**:203-218
- [17] Sasaki T, Ikegami M, Abe T, Miyazaki D, Kajikawa S, Naka Y. Real-time dynamic hologram in photorefractive ferroelectric liquid crystals with two-beam coupling gain coefficient of over 800 cm^{-1} and response time of 8 ms. *Applied Physics Letters*. 2013;**102**(1-6):063306
- [18] Sasaki T, Yoshino M, Naka Y, Le KV, Sassa T. Laser irradiation durability of photorefractive ferroelectric liquid

crystal blends containing terthiophene
photoconductive chiral dopants. RSC
Advances. 2016;**6**:70573-70580

[19] Sasaki T, Morino S, Sumiya A,
Yamamoto Y, Nakano M, Le KV, et al.
Enhancement of photosensitivity of
photorefractive ferroelectric liquid
crystal blends to green and red
wavelength regions using
oligothiophene photoconductive
dopants. Journal of Physical Chemistry
C. 2017;**121**:16951-16958

IntechOpen